Dual origin of ferropericlase inclusions within super-deep diamonds

Sofia Lorenzon [a,*], Michelle Wenz [b], Paolo Nimis [a], Steven D. Jacobsen [b],
Leonardo Pasqualetto [a], Martha G. Pamato [a], Davide Novella [a], Dongzhou Zhang [c],
Chiara Anzolini [d], Margo Regier [d], Thomas Stachel [d], D. Graham Pearson [d],
Jeffrey W. Harris [e], Fabrizio Nestola [a]

[a] *Department of Geosciences, University of Padua, Via G. Gradenigo 6, 35131 Padua, Italy*
[b] *Department of Earth and Planetary Sciences, Northwestern University, 2145 Sheridan Rd., Evanston, IL 60208, USA*
[c] *Hawaii Institute of Geophysics and Planetology, University of Hawaii, 1680 East-West Road, Honolulu, HI 96822, USA*
[d] *Department of Earth and Atmospheric Sciences, University of Alberta, AB T6G2E3 Edmonton, Canada*
[e] *School of Geographical and Earth Sciences, University of Glasgow, G12 8QQ Glasgow, United Kingdom*

ARTICLE INFO

ABSTRACT

Ferropericlase [(Mg,Fe)O] is one of the major constituents of Earth's lower mantle and the most abundant mineral inclusion in sub-lithospheric diamonds. Although a lower mantle origin for ferropericlase inclusions has often been suggested, some studies have proposed that many of these inclusions may instead form at much shallower depths, in the deep upper mantle or transition zone. No straightforward method exists to discriminate ferropericlase of lower-mantle origin without characteristic mineral associations, such as co-existing former bridgmanite. To explore ferropericlase-diamond growth relationships, we have investigated the crystallographic orientation relationships (CORs), determined by single-crystal X-ray diffraction, between 57 ferropericlase inclusions and 37 diamonds from Juina (Brazil) and Kankan (Guinea). We show that ferropericlase inclusions can develop specific (16 inclusions in 12 diamonds), rotational statistical (9 inclusions in 7 diamonds) and random (32 inclusions in 25 diamond) CORs with respect to their diamond hosts. All measured inclusions showing a specific COR were found to be Fe-rich ($X_{FeO} > 0.30$). Coexistence of non-randomly and randomly oriented ferropericlase inclusions within the same diamond indicates that their CORs may be variably affected by local growth conditions. However, the occurrence of specific CORs *only* for Fe-rich inclusions indicates that Fe-rich ferropericlases have a distinct genesis and are syngenetic with their host diamonds. This result provides strong support for a dual origin for ferropericlase in Earth's mantle, with Fe-rich compositions likely indicating redox growth in the upper mantle, while more Mg-rich compositions with random COR mostly representing ambient lower mantle trapped as protogenetic inclusions.

© 2023 Elsevier B.V. All rights reserved.

1. Introduction

Diamonds are the only natural samples through which we can investigate the mineralogy and geological processes occurring in Earth's mantle at depths down to ∼800 km depth. Most infor-

mation is provided by mineral and fluid inclusions entrapped by diamonds during their crystallization (Meyer, 1987; Shirey et al., 2019, 2013; Weiss et al., 2015). Ferropericlase, an oxide mineral with composition ranging from MgO (periclase) to wüstite (FeO), is the most abundant inclusion in super-deep diamonds, i.e., forming at sub-lithospheric depths. Experiments and theoretical models on pyrolitic compositions indicate that ferropericlase is stable in the lower mantle, at depths between ∼660 and 2900 km, and represents ∼17% of the mantle phase assemblage in a "fertile" mantle bulk composition, the remainder being represented by bridgmanite (76%) and CaSiO$_3$-perovskite (7%) (Akaogi, 2007; Ishii et al., 2018). The predicted chemical composition of lower-mantle ferropericlase is Mg-rich, with X_{FeO} (FeO molar fraction) ranging from 0.08 to 0.18 (Hirose, 2002; Irifune, 1994; Ishii et al., 2018, 2011; Kuwahara et al., 2018). Ferropericlase, however, represents ∼42% of the

inclusions reported within super-deep diamonds, far more abundant and showing much more variable compositions with X_{FeO} up to 0.85 than would be expected for pyrolitic mantle (Walter et al., 2022 and references therein).

Numerous studies (see Walter et al., 2022 for a review) tried to explain these discrepancies and unravel the possible geological processes involved in formation of ferropericlase-bearing diamonds. Assuming that ferropericlase-bearing diamonds crystallized in the lower mantle, Liu (2002) proposed a model according to which (Fe-rich) ferropericlase and diamond can simultaneously precipitate through decarbonation of $(Mg,Fe)CO_3$. Alternatively, Ryabchikov and Kaminsky (2013) and Kaminsky and Lin (2017) supposed the existence of a non-pyrolitic source in the lower mantle. However, experiments demonstrate that ferropericlase can be stable in mantle rocks at depths shallower than the lower mantle (Brey et al., 2004). In particular, Thomson et al. (2016) showed that ferropericlase with variable Fe contents plus diamond can crystallize simultaneously by interaction between mantle peridotite and slab-derived carbonatite melts in the deep upper mantle or transition zone. Therefore, in the absence of limiting characteristic mineral associations, such as the presence of former bridgmanite, the depth of origin of ferropericlase-bearing diamonds remains uncertain. Only inclusions associated with low-Ni enstatite, considered to be the back-transformation product of bridgmanite (Stachel et al., 2000), can safely be ascribed to the lower mantle. About 15% of these also co-exist with $MgSiO_3$ or/and $CaSiO_3$ phases in diamonds (Walter et al., 2022).

Determining ferropericlase-diamond growth relationships, for instance whether the inclusion and host crystallized simultaneously or whether the inclusion preceded the host, is crucial for determining the possible genetic processes that formed ferropericlase-bearing diamonds. Determination of crystallographic orientation relationships (CORs) for inclusion-diamond systems is commonly used to derive information about their growth relationships (Milani et al., 2016; Nestola et al., 2019, 2017, 2014, Nimis et al., 2019, 2018; Pamato et al., 2021; Pasqualetto et al., 2022). In a preliminary study, Nimis et al. (2018) determined CORs for nine Fe-rich ($X_{FeO} \approx 0.33$ to ≥ 0.64) ferropericlase inclusions in two diamonds from Juina, Brazil. These inclusions are *specifically* oriented with their diamond hosts, with the principal crystallographic axes of ferropericlase fixed to those of the diamond host, suggesting an epitaxial relationship. Accordingly, Nimis et al. (2018) proposed that such ferropericlase nucleated during the growth history of the diamond, probably by the same type of redox reactions investigated by Thomson et al. (2016) at depths of the deep upper mantle or transition zone.

In order to increase the statistical significance of the data and to gain further insight into ferropericlase-diamond growth relationships, we have determined the CORs for 57 ferropericlase inclusions in 37 diamonds spanning a large compositional range to determine possible associations between ferropericlase Fe-content and the depth origins of ferropericlase-bearing diamonds.

2. Samples and methods

2.1. Samples

In this work, we investigated 57 ferropericlase inclusions within 37 diamonds from two classic super-deep diamond localities. A representative example of one of these diamonds is shown in Fig. 1. Of the investigated samples, 34 diamonds with 49 inclusions in total come from Juina, Brazil, and 3 diamonds with 8 inclusions in total come from Kankan, Guinea. All the studied diamonds come from alluvial deposits. They are colourless to pale yellow-brown and their size ranges from ~1.5 to 5 mm. They show octahedral to irregular shapes and contain from one to four optically visible and

Fig. 1. One of the studied ferropericlase-bearing diamonds (*AZ*_08) under incident light. This specific sample comes from Juina (Brazil), is pale-yellow and has an elongated irregular shape. The ferropericlase inclusion (within the red circle and indicated by the red arrow) is dark in colour and ~250 μm sized.

measurable ferropericlase inclusions. The ferropericlase inclusions, are sub-rounded to irregular, 50-200 μm in size, dark in colour and show characteristic iridescence. In some specimens, other mineral and fluid phases also occur (such as calcite, dolomite, magnesite, nahcolite, olivine, breyite and a fluid phase similar to that reported in Nimis et al., 2016).

2.2. Single-crystal X-ray diffraction

X-ray diffraction data for 24 ferropericlase inclusions and 18 diamonds were collected using a Rigaku Oxford SuperNova diffractometer located at the Department of Geosciences, University of Padua. This instrument is equipped with a Dectris Pilatus 200 K area detector and a *Mova* X-ray micro source, operating at 50 kV and 0.8 mA. The detector distance is 68 mm and the diffractometer is controlled by the Crysalis-PRO^{TM} software. Initially, each ferropericlase inclusion was centred optically and subsequently more precisely aligned by X-ray diffraction. The diffraction data were collected in 360° phi-scan mode. Each frame width was 1° and the exposure time was 25-60 s per frame, as a function of the inclusion size. The Crysalis-PRO^{TM} software was also used to process the collected data. By indexing the position of the diffracted peaks from the inclusions and the hosts, we determined their orientation matrices, which represent the inclusion or host orientation relative to the reference system of the diffractometer. Through the indexing procedure, we could unambiguously distinguish diffraction peaks from ferropericlase apart from those of diamond in the same data set.

The remaining 33 ferropericlase inclusions within 19 diamonds were analysed at the single-crystal X-ray diffraction beamline (13-BM-C) of the GeoSoil Enviro Center for Advanced Radiation Sources (GSECARS), Advanced Photon Source (APS), Argonne National Laboratory, USA. For the synchrotron X-ray diffraction experiments, centring ferropericlase inclusions in diamond was facilitated using the 2D radiography attachment on beamline 13-BM-C (Wenz et al., 2019). For diffraction, the X-ray beam was focused to 12 μm horizontal by 18 μm vertical at full-width half-maximum. Final centring and diffraction were carried out on the six-circle goniometer following the methods detailed in Zhang et al. (2017). Step scans were obtained with one-degree steps over 180° with an exposure time of one second per step using a MAR 165 CCD detector. Additional details about the combined 2D radiography and synchrotron X-ray diffraction data collection and software are reported in Wenz et al. (2019).

2.3. COR determination: OrientXplot software and misorientation distribution analysis

The OrientXplot software (Angel et al., 2015) was used to determine and plot the CORs. This program processes each orientation matrix and displays a stereogram of the crystallographic orientations of inclusions relative to their host, avoiding ambiguities arising from crystal symmetry. In this case, both inclusions and hosts are cubic. Consequently, for each ferropericlase-diamond pair, 576 symmetrically equivalent orientations are possible. Therefore, for each inclusion-host pair, we have chosen to plot the orientation for which $[1\ 1\ 0]_{FPer}$ is closest to $[1\ 1\ 0]_{Dia}$ and $[0\ 0\ 1]_{FPer}$ is closest to $[0\ 0\ 1]_{Dia}$.

In order to determine the statistical significance of CORs in our inclusion-host systems, we carried out a misorientation distribution analysis. For this purpose, we considered the angles between the crystallographic axes or planes of ferropericlase and diamond that are the most likely to form non-random CORs (e.g., Nimis et al., 2019; Pasqualetto et al., 2022). The calculated misorientation distributions were compared with a theoretical model of 2 million randomly oriented matrices through the Kolmogorov-Smirnov test for two samples (see Wheeler et al., 2001 for more information). Identification of specific, rotational statistical or random CORs was then based on the presence or not of a statistically significant similarity between one or more pairs of specific crystallographic directions of inclusions and hosts (Griffiths et al., 2016; Habler and Griffiths, 2017).

To increase the number of data and the statistical significance, the same procedures were extended to include also two ferropericlase inclusions in diamond $AZ1$ previously studied by Anzolini et al. (2019).

2.4. Ferropericlase chemical composition

The chemical compositions of three ferropericlase inclusions (inclusions in samples AZ_08, AZ_15 and AZ_20) were determined using a Tescan Solaris dual beam FE-SEM, equipped with an Ultim® Max 65 EDS spectrometer. Analytical conditions were 15 keV, 3 nA, and 20 s counting time. Analyses were standardised using pure oxides as standards, excepting Na, which was calibrated on albite. In addition, the chemical data of four ferropericlase inclusions within $KK207$ diamond were collected by electron probe micro-analysis using a JEOL JXA-8900R with 5 wavelength dispersive spectrometers, located at the University of Alberta. The beam energy was 20 keV energy with 30 nA of beam current and 2 μm diameter. The counting time was 20 seconds for Si Kα, Fe Kα, Mn Kα, Ni Kα, Zn Kα, 30 seconds for V Kα, Ti Kα, Cr Kα, 40 seconds for Na Kα, K Kα, Ca Kα, Mg Kα, and 120 seconds for Al Kα.

3. Results

3.1. Crystallographic orientation relationships (CORs)

A COR is defined as a systematic relation between the crystallographic orientations in an inclusion-host system. Four types of CORs can be distinguished based on the degrees of freedom between inclusion and host orientations: specific, rotational statistical, dispersional statistical and random (Griffiths et al., 2016; Habler and Griffiths, 2017). This classification is only descriptive and independent from the mechanisms of their formation. In specific CORs, at least two crystallographic directions of the inclusion are fixed to the host (0 degrees of freedom). In rotational statistical CORs, only one inclusion crystallographic orientation is fixed to that of the host (1 degree of freedom). In dispersional statistical CORs, an inclusion crystallographic direction is not exactly fixed to the host, but is dispersed around it within a certain misorientation
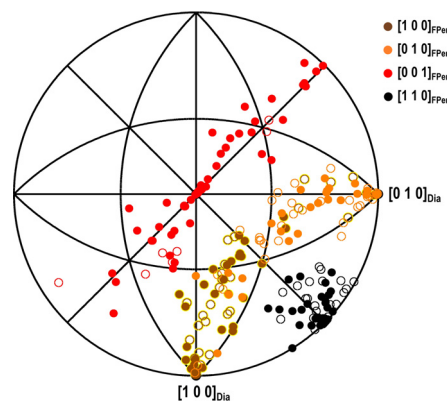

Fig. 2. Crystallographic orientation relationships (CORs) between all analysed 57 ferropericlase inclusions and their 37 diamond hosts, plotted using OrientXplot software (Angel et al., 2015). Open symbols plot in the lower hemisphere.

angle range (2 degrees of freedom, but within strict limits). In all other cases, the inclusion crystallographic directions are randomly oriented relative to the host (2 degrees of freedom, with no limit).

The CORs for all the 57 analysed ferropericlase inclusions are shown in Fig. 2. Sixteen inclusions have the three principal crystallographic axes (a_1, a_2, a_3) within 0-12° of those of their diamond hosts (Fig. 3a). Despite the angular mismatch being in some cases greater than the measurement uncertainties of ±4° (Nimis et al., 2019), all inclusions have their $[1\ 1\ 2]$ axis within uncertainty of $[1\ 1\ 2]_{Dia}$ at $< \pm4°$. These results are similar to those reported by Nimis et al. (2018) on nine ferropericlase inclusions in two diamonds. As suggested by Nimis et al. (2018), the small angular misorientation of the main crystallographic axes may be due to a slight rotation around the $[1\ 1\ 2]$ direction, caused by post-entrapment plastic deformation, which is well documented in super-deep diamonds (e.g. Agrosì et al., 2017; Howell et al., 2012). All these inclusions are thus interpreted to have been *specifically* oriented at the time of their incorporation. Another nine inclusions have their $[1\ 1\ 0]$ direction almost parallel (within ±4°) to $[1\ 1\ 0]_{Dia}$ and the other crystallographic directions randomly rotated around this axis (Fig. 3b). These relationships indicate a rotational statistical COR. The remaining inclusions (32 inclusions in 25 diamonds) do not show any particular crystallographic orientation with respect to their hosts (Fig. 3c). The statistical significance of the observed specific and rotational statistical CORs was tested by comparing the observed misorientation angle distributions against a theoretical random distribution (Kolmogorov-Smirnov test for two samples, $p < 0.001$).

Diamonds containing more than one ferropericlase inclusion (13 out of 37 diamonds) showed further interesting features. In three of these samples ($5a08$, $5a26$, $5a27$), inclusions that are specifically oriented coexist with others that are randomly oriented (Fig. 4a). Diamond $5a06$ contains one specifically oriented inclusion and one that suggests a rotational statistical COR (Fig. 4b). In diamonds $5a04$ and $6b23$, one inclusion with a rotational statistical COR and one randomly oriented inclusion coexist (Fig. 4c). Finally, in four diamonds ($KK34$, $KK207$, $6a05$, $6b17$) more than one inclusion share a similar orientation, but they are randomly oriented relative to their diamond hosts (Fig. 5).

3.2. Ferropericlase chemical composition

The chemical compositions of ferropericlase inclusions in diamond AZ_08 (1 inclusion), AZ_15 (1 inclusion), AZ_20 (1 inclusion) and $KK207$ (4 inclusions) are reported in Table 1. The X_{FeO} fraction ranges from 0.14 to 0.32. Previous data for other crystallographically analysed ferropericlase inclusions in diamonds studied
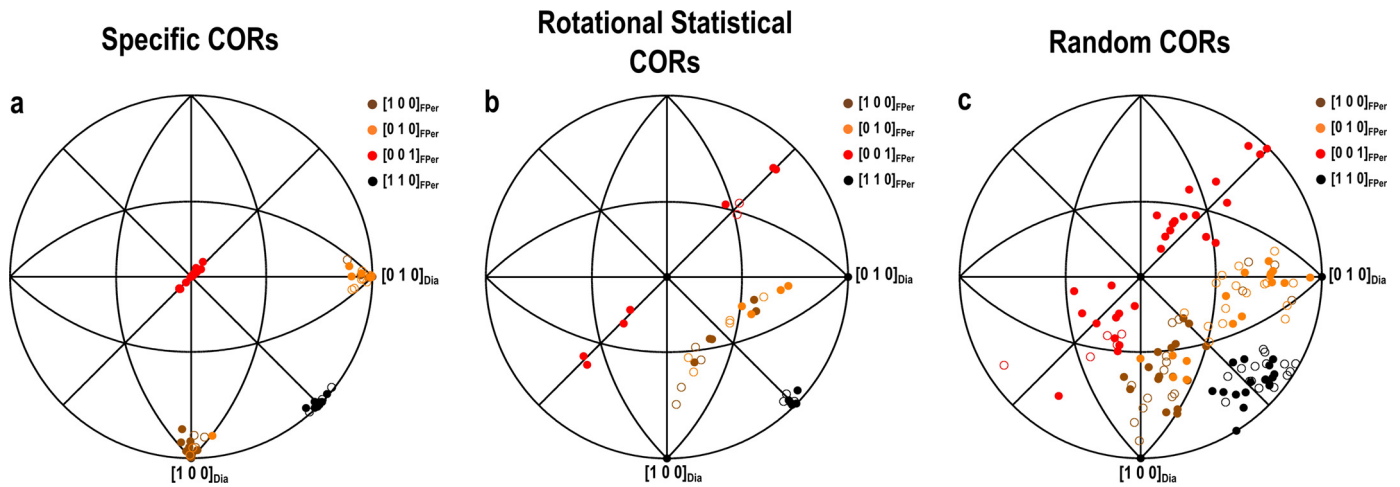
Fig. 3. Stereographic projections showing ferropericlase inclusions presenting a) specific COR (16 inclusions in 12 diamonds), b) rotational statistical COR ([1 1 0]$_{FPer}$ // [1 1 0]$_{Dia}$, 9 inclusions in 7 diamonds) and c) random CORs (32 inclusions in 25 diamonds) relative to their diamond hosts.
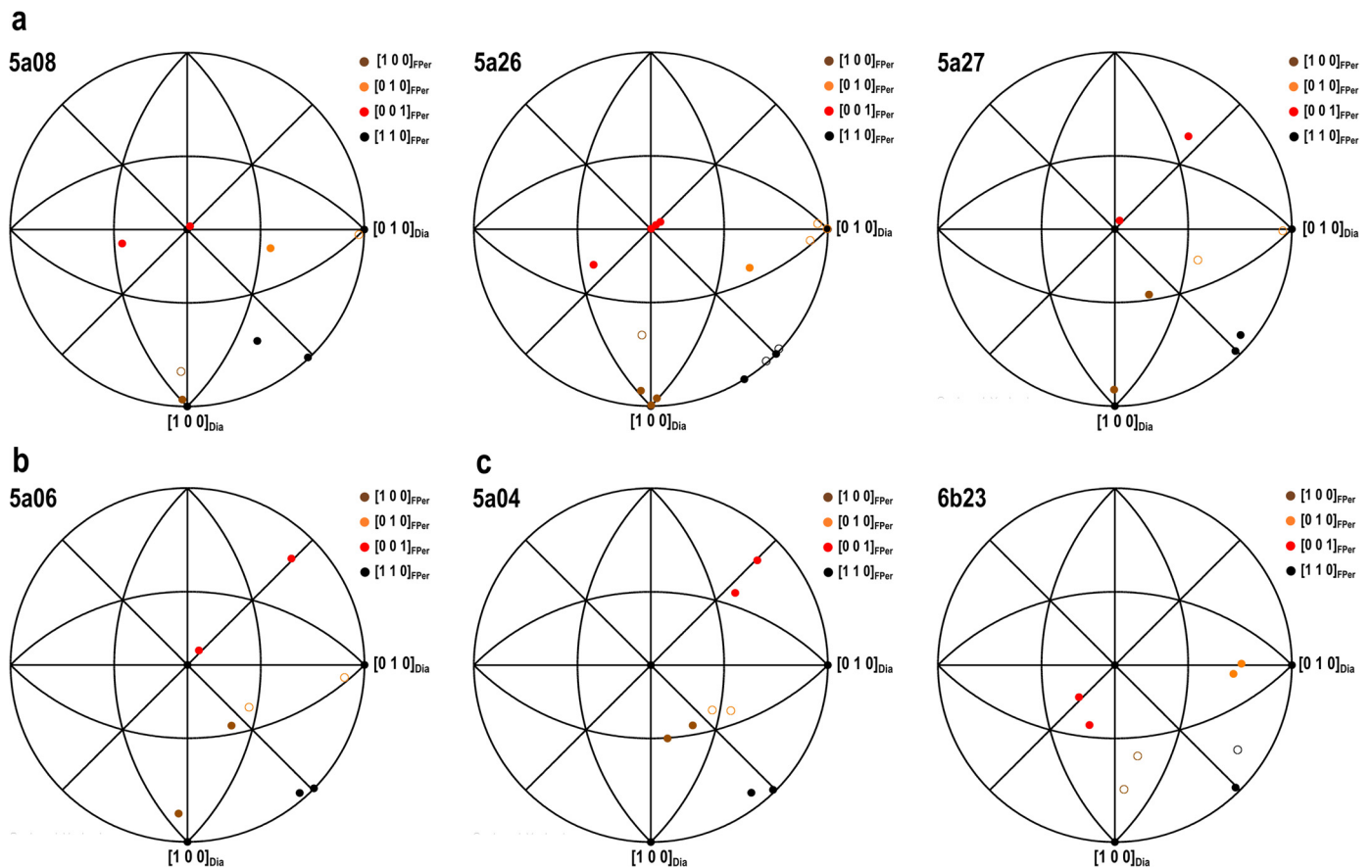

Fig. 4. Stereographic projections of diamonds containing ferropericlase inclusions which present a) both specific and random CORs (5a08, 5a26, 5a27), b) both specific and rotational statistical CORs (5a06) and c) both rotational statistical and random CORs (5a04, 6b23) relative to their diamond hosts.

by (Anzolini et al., 2019) and Nimis et al. (2018) are reported in the same Table.

4. Discussion

Our analysis of 57 ferropericlase inclusions within 37 diamonds shows that ferropericlase can develop specific (16 inclusions in 12 diamonds), rotational statistical (9 inclusions in 7 diamonds) and random (32 inclusions in 25 diamonds) CORs with respect to their diamond hosts. Non-random (i.e., specific and rotational statistical) CORs indicate that mechanical or surface interaction oc-

curred between ferropericlase and diamond during formation of the inclusion-host system (Habler and Griffiths, 2017; Wheeler et al., 2001). Mechanical juxtaposition of two well-shaped crystals is most likely to generate rotational statistical CORs, in which the two crystals share the axes normal to the juxtaposed faces (Nimis et al., 2019; Wheeler et al., 2001). In our samples characterised by rotational statistical COR, ferropericlase and diamond share a common [1 1 0] axis. If the driving force for this COR was mechanical, this would imply juxtaposition of the {1 1 0} faces of both minerals. Although ferropericlase and diamond can rarely develop {1 1 0}
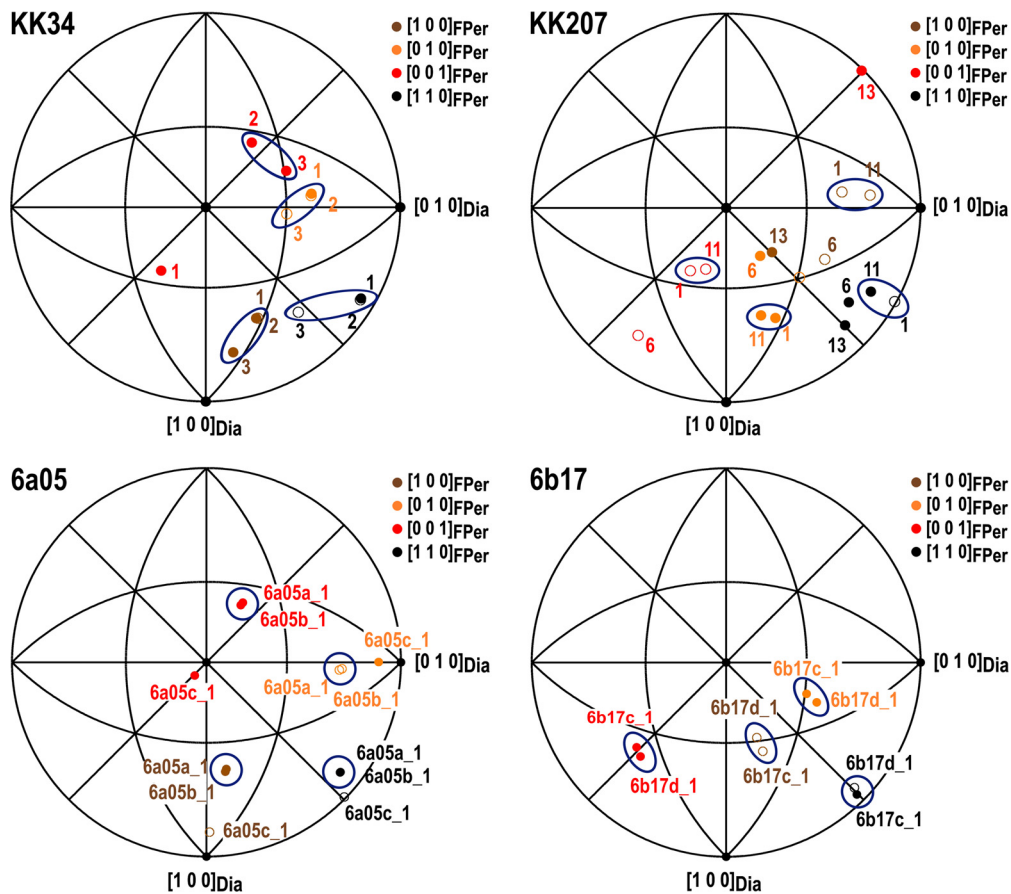
Fig. 5. Crystallographic orientation relationships (CORs) of ferropericlase inclusions within $KK34$, $KK207$, $6a05$ and $6b17$ diamonds. Multiple ferropericlase inclusions are defined by the numbers close to dots (i.e. 1, 2,...). Blue circles indicate the ferropericlase inclusions presenting similar orientations, but different and random CORs to their diamond host. These inclusions are protogenetic, representing remnant parts of pre-existing mono-crystals that were dissolved and entrapped during diamond precipitation.

Table 1
Chemical composition and interpreted COR of ferropericlase inclusions.

	Diamond	Inclusion	Chemical composition	Type of COR
Nimis et al., 2018	BZ270	1	$(Mg_{0.66}Fe_{0.34})O$	Specific
		2	$(Mg_{0.65}Fe_{0.35})O$	Specific
		3	$(Mg_{0.65}Fe_{0.35})O$	Specific
		4	$(Mg_{0.65}Fe_{0.35})O$	Specific
		5	$(Mg_{0.66}Fe_{0.34})O$	Specific
	JUc4	1	$(Mg_{0.43}Fe_{0.57})O$	Specific
		2	$(Mg_{0.56}Fe_{0.44})O$	Specific
		3	$(Mg_{0.57}Fe_{0.43})O$	Specific
		4	$(Mg_{0.36}Fe_{0.64})O$	Specific
Anzolini et al., 2019	AZ1	AZ1_1	$(Mg_{0.61}Fe_{0.39})O$	Specific
		AZ1_2	$(Mg_{0.59}Fe_{0.41})O$	Specific
This study	AZ_08	AZ_08_01	$(Mg_{0.68}Fe_{0.32})O$	Random
	AZ_15	AZ_15_01	$(Mg_{0.80}Fe_{0.20})O$	Random
	AZ_20	AZ_20_01	$(Mg_{0.69}Fe_{0.31})O$	Specific
	KK207	1	$(Mg_{0.86}Fe_{0.14})O$	Random
		6	$(Mg_{0.86}Fe_{0.14})O$	Random
		11	$(Mg_{0.86}Fe_{0.14})O$	Random
		13	$(Mg_{0.86}Fe_{0.14})O$	Rotational statistical?

faces during their growth (Koretsky et al., 1998; Sunagawa, 1990), their crystals commonly have octahedral habits with well-formed {1 1 1} faces. Consequently, one would expect to observe frequent rotational statistical CORs around [1 1 1] and not around [1 1 0]. Therefore, we do not favour a role of mechanical interaction in the development of rotational statistical CORs in our samples.
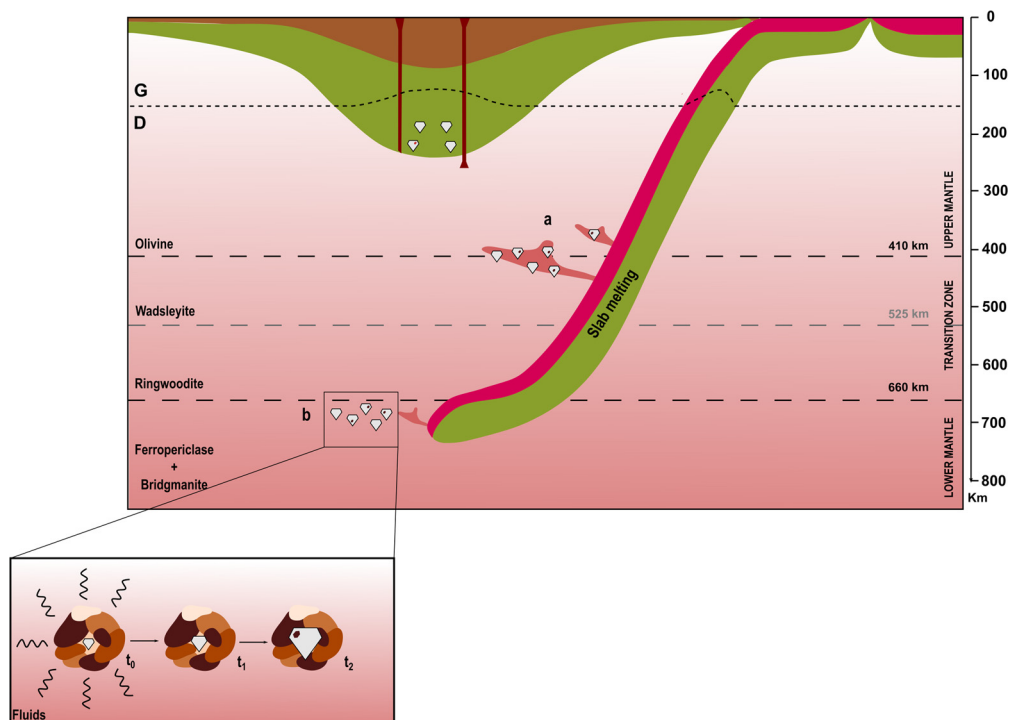
Fig. 6. Possible scenarios for the formation of Fe-rich and Fe-poor ferropericlase-bearing diamonds in Earth's mantle. a) Precipitation of diamonds and Fe-rich ferropericlase due to reactions between slab-derived carbonatite melts and peridotitic rocks, at depths of the deep upper mantle or of the transition zone (Thomson et al., 2016). In this case, the ferropericlase inclusions are syngenetic and generally develop specific CORs with their diamond hosts. b) Formation of diamonds in the uppermost lower mantle. In this case, pre-existing Mg-rich ferropericlase inclusions are partially dissolved and passively incorporated into the growing diamonds, without development of particular CORs. Multiple inclusions in individual diamonds may be iso-oriented if they are derived from the same original ferropericlase grain. Only in this case do the inclusions have chemical compositions similar to those experimentally predicted for ferropericlase in the lower mantle.

Surface interaction may also cause the development of non-random CORs (Wheeler et al., 2001). In fact, under favourable conditions, two mineral grains may align their crystal lattices or one of their lattice directions to minimize their interface energy. Nimis et al. (2018) discussed the possible scenarios that could lead to crystallographic alignment between inclusion and host by surface interaction in super-deep diamonds. These scenarios include (1) grain rotation during static recrystallization, or (2) mutual growth or epitaxial nucleation during crystallization from a fluid or melt. Scenario 1 was considered to be highly unlikely, given the high-stress environment in which super-deep diamonds form. Scenario 2 implies precipitation of the included minerals during the growth history of diamond and we suggest may apply to all investigated ferropericlase-diamond pairs showing non-random CORs.

Coexistence of non-random and random CORs in some of the studied diamonds (Fig. 4) is not in conflict with the above interpretation, since local physical-chemical and stress conditions may affect the efficiency of surface interactions (Mutaftschiev, 2001; Wheeler et al., 2001). Therefore, the absence of a non-random COR should not be considered as evidence against contemporaneous growth. Also, a rotational statistical CORs could reflect a "starting preferred crystallographic orientation" between ferropericlase and diamond. This would explain the coexistence in some of our samples of rotational statistical and either specific or random CORs within the same diamond.

Four diamonds each contain pairs of ferropericlase inclusions, which are iso-oriented with respect to each other, but are randomly oriented with respect to their diamond hosts (Fig. 5). In one of these, diamond 6b17, $[1\ 1\ 0]_{FPer}$ is 4° from $[1\ 1\ 0]_{Dia}$, but this relatively small misalignment may well represent just one of an infinite number of possible random orientations. Inclusion iso-orientation without a specific COR with the diamond host is considered to be evidence of a protogenetic origin of the inclu-

sions (Milani et al., 2016; Nestola et al., 2014; Nimis et al., 2019; Pamato et al., 2021; Pasqualetto et al., 2022).

Our compilation of ferropericlase inclusions for which both CORs and chemical data are available (Anzolini et al., 2019; Nimis et al., 2018; and present study) (Table 1) indicates a strong relationship between ferropericlase Fe content and ferropericlase-diamond growth relationships. Almost all (12 out of 13) Fe-rich ferropericlase inclusions ($X_{FeO} > 0.3$) present a specific COR. Evaluating the relationship between the Fe-rich composition of ferropericlase and the development of a specific COR through a non-parametric statistical test (Fisher's exact test), we have obtained very low probabilities ($p < 0.001$) that the presence of this specific COR is independent from the Fe-rich composition of ferropericlase within the studied population. This indicates that the association between these two variables is highly statistically significant. On the other hand, 4 out of 5 Mg-rich ferropericlase inclusions with $X_{FeO} \leq 0.2$ present random CORs, while the remaining one is compatible with both a random and a rotational statistical COR. In diamond KK207, multiple Mg-rich inclusions show evidence of a protogenetic origin (Fig. 5). These results strongly suggest that Fe-rich and Fe-poor ferropericlases generally form by distinct processes under distinct conditions.

The compositions of the Fe-rich ferropericlase inclusions ($X_{FeO} = 0.31$-0.57) are within the wide range predicted for diamond-associated ferropericlases produced by carbonate melt-peridotite reactions in the deep upper mantle or transition zone Thomson et al. (2016). The Mg-rich ferropericlase inclusions have chemical compositions similar to those of ferropericlases in experiments on pyrolitic and harzburgitic systems at lower-mantle conditions ($X_{FeO} < 0.2$; Hirose, 2002; Irifune, 1994; Ishii et al., 2011, 2018; Kuwahara et al., 2018 or found in association with former bridgmanite within diamonds (n= 40, range =∼ 0.10–0.31 and one sample having $X_{FeO} \sim 0.35$, median = 0.17; Hutchison, 1997;

Davies et al., 1999, 2004; Harte and Harris, 1994; Hayman et al., 2005; Stachel et al., 2000; Tappert et al., 2009). Accordingly, we suggest that Fe-rich ferropericlase inclusions, which frequently present a specific COR, are syngenetic with their diamond hosts and were formed in the deep upper mantle or transition zone by redox processes similar to those reproduced in Thomson et al.'s (2016) experiments (Fig. 6a). Conversely, Mg-rich ferropericlase inclusions, which present random CORs, and in some cases show clear evidence of protogenesis, represent parts of pre-existing mineral assemblages, which were partially dissolved and passively entrapped by diamond during its precipitation in the lower mantle (Fig. 6b). These results thus allow future geochemical studies of ferropericlase to confidently distinguish those formed at relatively shallow mantle levels by slab mantle interaction from those likely present in the upper mantle before diamond crystallization and entrapment. The observed relationships indicate that Fe-rich ferropericlase is unlikely to reflect a typical upper or lower mantle composition.

5. Conclusions

The results of this study can be summarised as follows.

1) The determination of the relative crystallographic orientations of 57 ferropericlase inclusions in 37 diamonds revealed the occurrence of specific, rotational statistical and random CORs.
2) A non-random COR is typical of Fe-rich ($X_{FeO} > 0.3$) ferropericlase inclusions, whereas Fe-poor ($X_{FeO} < 0.3$) ferropericlase inclusions show random CORs and sometimes exhibit clear evidence of protogenesis.
3) Fe-rich ferropericlase inclusions presenting non-random CORs are interpreted to have been formed together with their host diamonds in the deep upper mantle or transition zone, probably by interaction of mantle peridotite with slab-derived carbonatite melts.
4) Mg-rich ferropericlase inclusions presenting random CORs could be remnants of pre-existing mineral assemblages, which were entrapped by the growing diamonds in the lower mantle.

The dual origin of ferropericlase inclusions in diamonds (Fe-poor protogenetic vs. Fe-rich syngenetic) provides a simple explanation for the observed discrepancies between theoretical mineralogical models for the lower mantle and the relative abundance and composition of ferropericlase inclusions in diamonds.

CRediT authorship contribution statement

Sofia Lorenzon: Conceptualization, Formal analysis, Investigation, Writing – original draft. **Michelle Wenz:** Formal analysis, Investigation, Writing – review & editing. **Paolo Nimis:** Conceptualization, Investigation, Writing – review & editing. **Steven D. Jacobsen:** Conceptualization, Funding acquisition, Writing – review & editing. **Leonardo Pasqualetto:** Formal analysis, Writing – review & editing. **Martha G. Pamato:** Funding acquisition, Writing – review & editing. **Davide Novella:** Funding acquisition, Writing – review & editing. **Dongzhou Zhang:** Investigation. **Chiara Anzolini:** Writing – review & editing. **Margo Regier:** Investigation. **Thomas Stachel:** Resources, Writing – review & editing. **D. Graham Pearson:** Resources, Writing – review & editing. **Jeffrey W. Harris:** Resources, Writing – review & editing. **Fabrizio Nestola:** Conceptualization, Funding acquisition, Resources, Supervision, Writing – review & editing.

Declaration of competing interest

The authors declare that they have no known competing financial interests or personal relationships that could have appeared to influence the work reported in this paper.

Data availability

Data are present as Supplementary files

Appendix A. Supplementary material

Supplementary material related to this article – files containing the UB-matrix data of both ferropericlases and diamonds and the chemical data expressed in oxide abundances of ferropericlase inclusions).

Supplementary material related to this article can be found online at https://doi.org/10.1016/j.epsl.2023.118081.

References

Agrosì, G., Tempesta, G., Della Ventura, G., Cestelli Guidi, M., Hutchison, M., Nimis, P., Nestola, F., 2017. Non-Destructive In Situ Study of Plastic Deformations in Diamonds: X-ray Diffraction Topography and μFTIR Mapping of Two Super Deep Diamond Crystals from São Luiz (Juina, Brazil). Crystals 7, 233. https://doi.org/10.3390/cryst7080233.

Akaogi, M., 2007. Phase transitions of minerals in the transition zone and upper part of the lower mantle. Spec. Pap., Geol. Soc. Am. 421, 1–13. https://doi.org/10.1130/2007.2421(01).

Angel, R., Milani, S., Alvaro, M., Nestola, F., 2015. OrientXplot: A program to analyse and display relative crystal orientations. J. Appl. Crystallogr. 48, 1330–1334. https://doi.org/10.1107/S160057671501167X.

Anzolini, C., Nestola, F., Mazzucchelli, M.L., Alvaro, M., Nimis, P., Gianese, A., Morganti, S., Marone, F., Campione, M., Hutchison, M.T., Harris, J.W., 2019. Depth of diamond formation obtained from single periclase inclusions. Geology 47, 219–222. https://doi.org/10.1130/G45605.1.

Brey, G.P., Bulatov, V., Girnis, A., Harris, J.W., Stachel, T., 2004. Ferropericlase - a lower mantle phase in the upper mantle. Lithos 77, 655–663. https://doi.org/10.1016/j.lithos.2004.03.013.

Davies, R.M., Griffin, W.L., O'Reilly, S.Y., 1999. Diamonds from the deep: pipe DO27, Slave craton, Canada. In: Gurney, J.J., Gurney, J.L., Pascoe, M.D., Richardson, S.H. (Eds.), The J.B. Dawson vol. In: Proc. 7th Internat. Kimberlite Conf., Red Roof Designs, Cape Town, pp. 148–155.

Davies, R.M., Griffin, W.L., O'Reilly, S.Y., Doyle, B.J., 2004. Mineral inclusions and geochemical characteristics of microdiamonds from the DO27, A154, A21, A418, DO18, DD17 and Ranch Lake kimberlites at Lac de Gras, Slave Craton, Canada. Lithos 77, 39–55. https://doi.org/10.1016/j.lithos.2004.04.016.

Griffiths, T.A., Habler, G., Abart, R., 2016. Crystallographic orientation relationships in host-inclusion systems: new insights from large EBSD data sets. Am. Mineral. 101, 690–705. https://doi.org/10.2138/am-2016-5442.

Habler, G., Griffiths, T.A., 2017. Crystallographic orientation relationships. EMU Notes Mineral. 16, 541–585.

Harte, B., Harris, J.W., 1994. Lower mantle mineral associations preserved in diamonds. Mineral. Mag. 58A, 384–385. https://doi.org/10.1180/minmag.1994.58A.1.201.

Hayman, P.C., Kopylova, M.G., Kaminsky, F.V., 2005. Lower mantle diamonds from Rio Soriso (Juina area, Mato Grosso, Brazil). Contrib. Mineral. Petrol. 149, 430–445. https://doi.org/10.1007/s00410-005-0657-8.

Hirose, K., 2002. Phase transitions in pyrolitic mantle around 670-km depth: implications for upwelling of plumes from the lower mantle. J. Geophys. Res., Solid Earth 107. https://doi.org/10.1029/2001jb000597. ECV 3-1-ECV 3-13.

Howell, D., Piazolo, S., Dobson, D.P., Wood, I.G., Jones, A.P., Walte, N., Frost, D.J., Fisher, D., Griffin, W.L., 2012. Quantitative characterization of plastic deformation of single diamond crystals: a high pressure high temperature (HPHT) experimental deformation study combined with electron backscatter diffraction (EBSD). Diam. Relat. Mater. 30, 20–30. https://doi.org/10.1016/j.diamond.2012.09.003.

Hutchison, M.T., 1997. Constitution of the deep transition zone and lower mantle shown by diamonds and their inclusions. Ph.D. thesis. University of Edinburgh, Edinburgh, UK. 660 p., and CD-ROM.

Irifune, T., 1994. Absence of an aluminous phase in the upper part of the Earth's lower mantle. Nature 370, 131–133. https://doi.org/10.1038/370131a0.

Ishii, T., Kojitani, H., Akaogi, M., 2011. Post-spinel transitions in pyrolite and Mg2SiO4 and akimotoite-perovskite transition in MgSiO$_3$: precise comparison by high-pressure high-temperature experiments with multi-sample cell technique. Earth Planet. Sci. Lett. 309, 185–197. https://doi.org/10.1016/j.epsl.2011.06.023.

Ishii, T., Kojitani, H., Akaogi, M., 2018. Phase relations and mineral chemistry in pyrolitic mantle at 1600–2200 °C under pressures up to the uppermost lower mantle: phase transitions around the 660-km discontinuity and dynamics of upwelling hot plumes. Phys. Earth Planet. Inter. 274, 127–137. https://doi.org/10.1016/j.pepi.2017.10.005.

Kaminsky, F.V., Lin, J.F., 2017. Iron partitioning in natural lower-mantle minerals: Toward a chemically heterogeneous lower mantle. Am. Mineral. 102, 824–832. https://doi.org/10.2138/am-2017-5949.

Koretsky, C.M., Sverjensky, D.A., Sahai, N., 1998. A model of surface site types on oxide and silicate minerals based on crystal chemistry: implication for site types and densities, multi-site adsorption, surface infrared spectroscopy, and dissolution kinetics. Am. J. Sci. 298, 349–438.

Kuwahara, H., Nomura, R., Nakada, R., Irifune, T., 2018. Simultaneous determination of melting phase relations of mantle peridotite and mid-ocean ridge basalt at the uppermost lower mantle conditions. Phys. Earth Planet. Inter. 284, 36–50. https://doi.org/10.1016/j.pepi.2018.08.012.

Liu, L., 2002. An alternative interpretation of lower mantle mineral associations in diamonds. Contrib. Mineral. Petrol. 144, 16–21. https://doi.org/10.1007/s00410-002-0389-y.

Meyer, H.O.A., 1987. Inclusions in diamond. In: Nixon, P.H. (Ed.), Mantle xenoliths. John Wiley & Sons, Chichester, pp. 501–522.

Milani, S., Nestola, F., Angel, R.J., Nimis, P., Harris, J.W., 2016. Crystallographic orientations of olivine in diamonds. Lithos 265, 312–316. https://doi.org/10.1016/j.lithos.2016.06.010.

Mutaftschiev, B., 2001. The Atomistic Nature of Crystal Growth. Springer-Verlag, Berlin, p. 368. https://doi.org/10.1007/978-3-662-04591-6.

Nestola, F., Jacob, D.E., Pamato, M.G., Pasqualetto, L., Oliveira, B., Greene, S., Perritt, S., Chinn, I., Milani, S., Kueter, N., Sgreva, N., Nimis, P., Secco, L., Harris, J.W., 2019. Protogenetic garnet inclusions and the age of diamonds. Geology 47, 431–434. https://doi.org/10.1130/G45781.1.

Nestola, F., Jung, H., Taylor, L.A., 2017. Mineral inclusions in diamonds may be synchronous but not syngenetic. Nat. Commun. 8, 6–11. https://doi.org/10.1038/ncomms14168.

Nestola, F., Nimis, P., Angel, R.J., Milani, S., Bruno, M., Prencipe, M., Harris, J.W., 2014. Olivine with diamond-imposed morphology included in diamonds. Syngenesis or protogenesis? Int. Geol. Rev. 56, 1658–1667. https://doi.org/10.1080/00206814.2014.956153.

Nimis, P., Alvaro, M., Nestola, F., Angel, R.J., Marquardt, K., Rustioni, G., Harris, J.W., Marone, F., 2016. First evidence of hydrous silicic fluid films around solid inclusions in gem-quality diamonds. Lithos 260, 384–389. https://doi.org/10.1016/j.lithos.2016.05.019.

Nimis, P., Angel, R.J., Alvaro, M., Nestola, F., Harris, J.W., Casati, N., Marone, F., 2019. Crystallographic orientations of magnesiochromite inclusions in diamonds: what do they tell us? Contrib. Mineral. Petrol. 174, 1–13. https://doi.org/10.1007/s00410-019-1559-5.

Nimis, P., Nestola, F., Schiazza, M., Reali, R., Agrosì, G., Mele, D., Tempesta, G., Howell, D., Hutchison, M.T., Spiess, R., 2018. Fe-rich ferropericlase and magnesiowüstite inclusions reflecting diamond formation rather than ambient mantle. Geology 47, 27–30. https://doi.org/10.1130/G45235.1.

Pamato, M.G., Novella, D., Jacob, D.E., Oliveira, B., Pearson, D.G., Greene, S., Afonso, J.C., Favero, M., Stachel, T., Alvaro, M., Nestola, F., 2021. Protogenetic sulfide inclusions in diamonds date the diamond formation event using Re-Os isotopes. Geology 49, 941–945. https://doi.org/10.1130/G48651.1.

Pasqualetto, L., Nestola, F., Jacob, D.E., Pamato, M.G., Oliveira, B., Perritt, S., Chinn, I., Nimis, P., Milani, S., Harris, J.W., 2022. Protogenetic clinopyroxene inclusions in diamond and Nd diffusion modeling—Implications for diamond dating. Geology XX, 1–5. https://doi.org/10.1130/g50273.1.

Ryabchikov, I.D., Kaminsky, F.V., 2013. The composition of the lower mantle: evidence from mineral inclusions in diamonds. Dokl. Earth Sci. 453, 1246–1249. https://doi.org/10.1134/S1028334X13120155.

Shirey, S.B., Cartigny, P., Frost, D.J., Keshav, S., Nestola, F., Nimis, P., Pearson, D.G., Sobolev, N.V., Walter, M.J., 2013. Diamonds and the geology of mantle carbon. Rev. Mineral. Geochem. 75, 355–421. https://doi.org/10.2138/rmg.2013.75.12.

Shirey, S.B., Smit, K.V., Pearson, D.G., Walter, M.J., Aulbach, S., Brenker, F.E., Bureau, H., Burnham, A.D., Cartigny, P., Chacko, T., Frost, D.J., Hauri, E.H., Jacob, D.E., Jacobsen, S.D., Kohn, S.C., Luth, R.W., Mikhail, S., Navon, O., Nestola, F., Nimis, P., Palot, M., Smith, E.M., Stachel, T., Stagno, V., Steele, A., Stern, R.A., Thomassot, E., Thomson, A.R., Weiss, Y., 2019. Diamonds and the Mantle Geodynamics of Carbon: Deep Mantle Carbon Evolution from the Diamond Record, Deep Carbon: Past to Present.

Stachel, T., Harris, J.W., Brey, G.P., Joswig, W., 2000. Kankan diamonds (Guinea) II: lower mantle inclusion parageneses. Contrib. Mineral. Petrol. 140, 16–27. https://doi.org/10.1007/s004100000174.

Sunagawa, I., 1990. Growth and morphology of diamond crystals under stable and metastable conditions. J. Cryst. Growth 99, 1156–1161.

Tappert, R., Foden, J., Stachel, T., Muehlenbachs, K., Tappert, M., Wills, K., 2009. The diamonds of South Australia. Lithos 112, 806–821. https://doi.org/10.1016/j.lithos.2009.04.029.

Thomson, A.R., Walter, M.J., Kohn, S.C., Brooker, R.A., 2016. Slab melting as a barrier to deep carbon subduction. Nature 529, 76–79. https://doi.org/10.1038/nature16174.

Walter, M.J., Thomson, A.R., Smith, E.M., 2022. Geochemistry of silicate and oxide inclusions in sublithospheric diamonds. Rev. Mineral. Geochem. 88, 393–450. https://doi.org/10.2138/rmg.2022.88.07.

Weiss, Y., McNeill, J., Pearson, D.G., Nowell, G.M., Ottley, C.J., 2015. Highly saline fluids from a subducting slab as the source for fluid-rich diamonds. Nature 524, 339–342. https://doi.org/10.1038/nature14857.

Wenz, M.D., Jacobsen, S.D., Zhang, D., Regier, M., Bausch, H.J., Dera, P.K., Rivers, M., Eng, P., Shirey, S.B., Pearson, D.G., 2019. Fast identification of mineral inclusions in diamond at GSECARS using synchrotron X-ray microtomography, radiography and diffraction. J. Synchrotron Radiat. 26, 1763–1768. https://doi.org/10.1107/S1600577519006854.

Wheeler, J., Prior, D.J., Jiang, Z., Spiess, R., Trimby, P.W., 2001. The petrological significance of misorientations between grains. Contrib. Mineral. Petrol. 141, 109–124. https://doi.org/10.1007/s004100000225.

Zhang, D., Dera, P.K., Eng, P.J., Stubbs, J.E., Zhang, J.S., Prakapenka, V.B., Rivers, M.L., 2017. High pressure single crystal diffraction at PX^2. J. Vis. Exp. 2017, 1–9. https://doi.org/10.3791/54660.